WILEY | Hindawi

Research Article

Torque System Modeling and Electromagnetic Coupling Characteristics Analysis of a Midpoint Injection Type Bearingless Permanent Synchronous Magnet Motor

Wenshao Bu [iD] and Hang Li

Information Engineering College, Henan University of Science and Technology, Luoyang 471023, China

Correspondence should be addressed to Wenshao Bu; wsbu@163.com

Taking the Midpoint Injection type Bearingless Permanent Magnet Synchronous Motor (MPI-BL-PMSM) as an object, to solve its problems of large torque pulsation and insufficient suspension force when adopting Midpoint Suspension Current Unilateral Injection (MPSC-UI), a Midpoint Suspension Current Bilateral Injection (MPSC-BI) solution is proposed. Based on the half-winding structure of MPI-BL-PMSM, and from the electromechanical energy conversion principle, the torque model for MPSC-BI solution is established. On this basis, the torque model for MPSC-UI method was derived. The correctness of the established torque mathematical models based on half-winding structure was verified through the finite element method (FEM), and the "dual-frequency" electromagnetic coupling characteristics of suspension current on electromagnetic torque were compared and analyzed from the perspectives of theoretical model and FEM simulation. The results indicate that the MPSC-BI method can effectively suppress or avoid the torque pulsation coupled by suspension current and can obtain about 1-time increase of controllable suspension force; the advantages of MPSC-BI solution in dynamic torque decoupling characteristics are demonstrated, while the only downside is that the coupling effect of torque current on radial suspension force is slightly greater than that of the MPSC-UI method.

1. Introduction

Due to the high-power density and efficiency, permanent magnet synchronous motor has been widely used in industrial fields [1]. To meet motor's long-term and high-speed operation needs, the magnetic bearing technology is widely developed [2, 3], but it still has problems such as high-power consumption of magnetic suspension on and limited critical speed [3]. The bearingless motor is a new magnetic suspension motor proposed based on the structural similarity between magnetic bearing and AC motor stator [3–5]. In contrast to magnetic bearing motor, the bearingless motor not only maintains the benefits of no friction and no mechanical noise but also has shorter shaft and higher critical speed. Consequently, it holds significant application promise in many fields, such as high-speed flywheel energy storage,

advanced manufacturing, aerospace, and life sciences [3, 6, 7]. The bearingless motor typically comprises two sets of windings, i.e., torque winding and suspension winding. Although the dual-winding structure facilitates to control currents independently, the existence of suspension winding reduces the motor's power density and also reduces the operation reliability. Therefore, the single-winding structure is considered a trend in the development of bearingless motors [3, 8, 9]. In single-winding structure bearingless motor, the torque and radial suspension force are simultaneously generated by controlling the torque- and suspension-current components within a single set of stator windings. The use of a single-winding structure can eliminate the need for insulation materials between two sets of stator windings; then the motor's structure can be simplified, and the leakage flux can be reduced also.

The single-winding structure of bearingless motor has various forms, such as multiphase windings, parallel windings, and midpoint injection windings. The multiphase bearingless motors often adopt five-phase or six-phase structures [11–12], mainly through current superposition to generate two sets of rotating magnetic fields with 1-pair poles difference. In literature [12], six-phase windings are connected as two sets of three-phase windings, the torque, and suspension currents are superimposed on two sets of three-phase windings to simultaneously control the torque and radial force. The authors of [12–14] introduced the dual-purpose nonvoltage (DPNV) winding structure of bearingless permanent magnet synchronous motor (BL-PMSM), which includes two types of structures: bridge-configured winding and parallel winding. The DPNV winding structure can eliminate the influence of the induced electromotive force of torque system on the end voltage of suspension inverter. The bridge-configured winding requires three single-phase inverters with isolated power sources, which increases the system's complexity and design cost. Asama and Chiba [15] proposed a novel single-winding structure for six-slot six-pole BL-PMSM; it simultaneously generates a four-pole rotating field and a four-pole alternating field through three concentrated coils, and it utilizes a three-phase inverter to control the suspension force and single-phase motor torque. Chiba et al. [9] proposed a single-winding BL-PMSM structure based on midpoint suspension current unilateral injection (MPSC-UI) and provided a very good idea for bearingless motor's single-winding design. For the suspension current is only injected into one half-winding of per-phase, the controllable suspension force is not big enough, and the fluctuation of torque is obvious. Why the suspension current causes torque ripple and how to improve controllable suspension force and reduce coupling torque pulsation are still issues that need further research. Reference [16] integrates the torque winding and suspension winding into a cohesive winding and then proposes a stator coreless axial magnetic field self-bearing motor structure, which can avoid the tradeoff between force and torque and is conducive to simplifying the control of torque and suspension force.

In this paper, the midpoint suspension current unilateral injection type bearingless permanent magnet synchronous motor (MPI-BL-PMSM) is taken as an object, and based on the current superposition idea, a midpoint suspension current bilateral injection (MPSC-BI) solution is investigated. Firstly, the structure and working principles of MPI-BL-PMSM are introduced. Then based on the half-winding structure of MPI-BL-PMSM, the torque mathematical models for two midpoint injection methods are derived, and from a theoretical perspective, the comparative analysis is conducted on the coupling effect of suspension current on torque. Finally, model validation and coupling performance comparison analysis are conducted using the finite element method (FEM). The research results have proved the performance advantages of the proposed MPSC-BI method in reducing torque pulsation.

2. Motor Structure and Working Principle

Figure 1 shows the schematic diagram of the fundamental structure of a 6-slot 4-pole single-winding BL-PMSM. The inner rotor structure with surface-mounted permanent magnet is adopted. The stator windings are evenly distributed in six stator slots, where U_1 and U_2 coils are connected in series to constitute the four-pole U-phase winding, V_1 and V_2 coils are connected in series to constitute the four-pole V-phase winding, and W_1 and W_2 coils are connected in series to constitute the four-pole W-phase winding.

Figure 2 shows the connection topology between the motor winding and the inverter, as well as a schematic diagram of the current reference direction. In this setup, "Inverter 1" is linked to the output terminals of the three-phase Y-type windings. The midpoint of each phase winding is extended and linked to "Inverter 2." As for Inverter 2, the U-phase output terminal is connected to the midpoint of stator U-phase winding, and the output terminals of the V-phase and W-phase are "cross connected" to the midpoints of the stator W-phase winding and the stator V-phase winding, respectively. The current provided to the three-phase stator winding by inverter 1 comprises two parts, including the three-phase torque current and the required suspension current of the upper half winding of each phase. After the three-phase symmetrical suspension current components provided by inverter 2 are injected into the midpoints of three-phase windings, they are equally divided and separately injected into the upper half-winding and lower half-winding of each phase in opposite directions. In Figure 2, i_{Tu}, i_{Tv}, and i_{Tw} denote the torque currents entering the three-phase windings, whereas i_{Su}, i_{Sv}, and i_{Sw} represent the three-phase suspended currents injected from the midpoint. During BL-PMSM operation, the torque current, together with the permanent magnet, generates a torque system magnetic field with a polar number of P_T and generates electromagnetic torque. Simultaneously, the suspension current generates a suspension magnetic field with a pole pair number of P_S. When the two magnetic fields meet the condition of "$P_T = P_S \pm 1$" and their electrical angular frequency and rotation direction are the same, stable and controllable radial suspension force can be generated.

Figure 3 shows the schematic diagram of suspension force generation principle of radial magnetic suspension force when injecting suspension current into the two "half-phase winding" of each phase from winding midpoints. In Figure 3, after the torque current and suspension current are superimposed in the stator windings, the torque system magnetic field with two pairs of poles and the suspension magnetic field with one pair of poles are formed. The superposition of torque magnetic field and suspension magnetic field in the air gap will enhance the air gap magnetic field at position "1" and weaken the air gap magnetic field at position "3." Then, according to Maxwell principles, a radial electromagnetic force will be generated along the x-axis direction, namely, radial controllable magnetic suspension force. By adjusting the magnitude and phase of the suspension current, the magnitude and phase of the radial magnetic suspension force can be freely controlled.
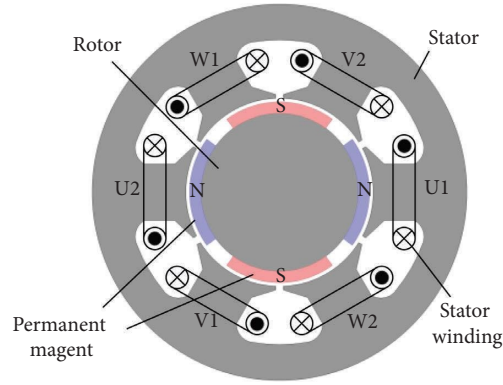
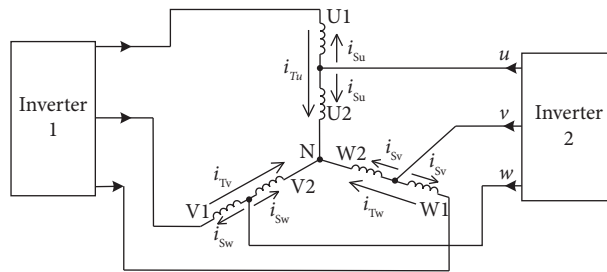FIGURE 1: Basic structure diagram of MPI-BL-PMSM.

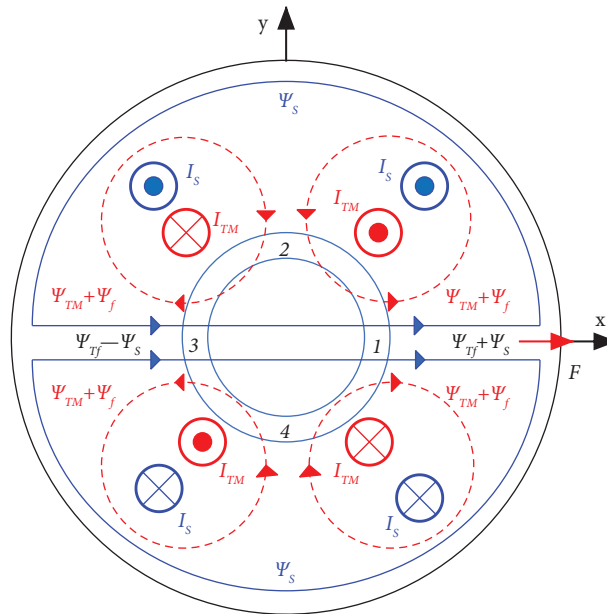FIGURE 2: Schematic diagram of winding connection topology under MPSC-BI.

FIGURE 3: Schematic diagram of suspension force generation principle for MPSC-BI method.

3. Torque System Modeling of MPI-BL-PMSM

3.1. Basic Mathematical Model of MPI-BL-PMSM. In this paper, the pole pair number of torque system magnetic field is $P_T = 2$, whereas the pole pair number corresponding to the suspension magnetic field is $P_S = 1$. When the MPSC-BI method is adopted, based on the current superposition concept, the current matrix of each coil (half-phase winding) that is ultimately fed from two inverters is expressed as follows:

$$
\begin{bmatrix} i_{u1} \\ i_{v1} \\ i_{w1} \\ i_{u2} \\ i_{v2} \\ i_{w2} \end{bmatrix} = \begin{bmatrix} i_{Tu} - i_{Su} \\ i_{Tv} - i_{Sw} \\ i_{Tw} - i_{Sv} \\ i_{Tu} + i_{Su} \\ i_{Tv} + i_{Sw} \\ i_{Tw} + i_{Sv} \end{bmatrix} = I_T \begin{bmatrix} \cos(\omega t + \varphi_T) \\ \cos\left(\omega t - \dfrac{2\pi}{3} + \varphi_T\right) \\ \cos\left(\omega t + \dfrac{2\pi}{3} + \varphi_T\right) \\ \cos(\omega t + \varphi_T) \\ \cos\left(\omega t - \dfrac{2\pi}{3} + \varphi_T\right) \\ \cos\left(\omega t + \dfrac{2\pi}{3} + \varphi_T\right) \end{bmatrix} + I_S \begin{bmatrix} \cos(\omega t - \pi + \varphi_S) \\ \cos\left(\omega t - \dfrac{\pi}{3} + \varphi_S\right) \\ \cos\left(\omega t + \dfrac{\pi}{3} + \varphi_S\right) \\ \cos(\omega t + \varphi_S) \\ \cos\left(\omega t + \dfrac{2\pi}{3} + \varphi_S\right) \\ \cos\left(\omega t - \dfrac{2\pi}{3} + \varphi_S\right) \end{bmatrix}, \tag{1}
$$

where I_T and I_S represent the amplitudes of torque current and suspension current, respectively, while φ_T and φ_S represent the initial phase angles of the torque current and suspension current, respectively.

The voltage equations of stator coils (half-phase windings) can be expressed in the following matrix form:

$$
U = Ri + \frac{d\psi}{dt}, \tag{2}
$$

where R represents the resistance matrix of each coil.

We define the self-inductance of each coil (i.e., half phase winding) and the mutual-inductance parameters in Figure 1 as follows:

(1) The self-inductance of each coil (i.e., each half phase winding) is L_1, $L_1 = L_{mf} + L_l$, where L_{mf} and L_l are the excitation inductance and leakage inductance of the half phase winding, respectively.

(2) The mutual inductance between adjacent coils is denoted as M_1 (such as that between U_1, V_2, and W_2).

(3) The mutual inductance between two coils with a spatial position difference of $180°$ is denoted as M_2 (such as that between U_1 and U_2).

(4) The mutual inductance between two coils with a spatial position difference of $120°$ is denoted as M_3 (such as that between U_1 and V_1 and W_1).

In addition, set α as the position electrical angle of permanent magnet rotor, $\alpha = \omega T$, and ψ_f as the phasor of magnetic flux-linkage generated by permanent magnet on a half-phase winding (stator coil). Then the magnetic flux of each half-phase winding can be expressed as follows:

$$
\psi = \begin{bmatrix} L_1 & M_3 & M_3 & M_2 & M_1 & M_1 \\ M_3 & L_1 & M_3 & M_1 & M_2 & M_1 \\ M_3 & M_3 & L_1 & M_1 & M_1 & M_2 \\ M_2 & M_1 & M_1 & L_1 & M_3 & M_3 \\ M_1 & M_2 & M_1 & M_3 & L_1 & M_3 \\ M_1 & M_1 & M_2 & M_3 & M_3 & L_1 \end{bmatrix} \begin{bmatrix} i_{u1} \\ i_{v1} \\ i_{w1} \\ i_{u2} \\ i_{v2} \\ i_{w2} \end{bmatrix} + \psi_f \begin{bmatrix} \cos(\omega t) \\ \cos\left(\omega t - \dfrac{2\pi}{3}\right) \\ \cos\left(\omega t - \dfrac{4\pi}{3}\right) \\ \cos(\omega t) \\ \cos\left(\omega t - \dfrac{2\pi}{3}\right) \\ \cos\left(\omega t - \dfrac{4\pi}{3}\right) \end{bmatrix}. \tag{3}
$$

From equations (2) and (3), the voltage equations for each half-phase winding can be derived. Taking U_1 and U_2 coils as example, the voltage equations are as follows:

$$
\begin{cases}
u_1 = Ri_{u1} + L_1 \dfrac{di_{u1}}{dt} + M_1 \dfrac{d(i_{v2} + i_{w2})}{dt} \\[2mm]
\quad + M_2 \dfrac{di_{u2}}{dt} + M_3 \dfrac{d(i_{v1} + i_{w1})}{dt} - P_T \omega_r \psi_f \sin \omega t, \\[3mm]
u_2 = Ri_{u2} + L_1 \dfrac{di_{u2}}{dt} + M_1 \dfrac{d(i_{v1} + i_{w1})}{dt} \\[2mm]
\quad + M_2 \dfrac{di_{u1}}{dt} + M_3 \dfrac{d(i_{v2} + i_{w2})}{dt} - P_T \omega_r \psi_f \sin \omega t.
\end{cases}
\tag{4}
$$

Consider the following current constraints: zero sum of three-phase torque currents and zero sum of three-phase suspension currents. According to Figure 2, when injecting torque current and bilateral suspension current into the stator winding, the U-phase voltage output by inverter 1 can be obtained from equation (4) as follows:

$$
U_{u1+u2} = u_1 + u_2 = 2Ri_{Tu} + 2(L_1 - M_1 + M_2 - M_3)
$$
$$
\cdot \frac{di_{Tu}}{dt} + 2 \frac{d\psi_f}{dt} - 2P_T \omega_r \psi_f \sin \omega t.
\tag{5}
$$

From equation (5), it can be seen that the output voltage of inverter 1 is solely determined by the torque current and not affected by suspension current. The reason is that when injecting bilateral suspension current from the midpoint of phase winding, the suspension currents in U_1 and U_2 half-phase windings are equal in magnitude and opposite in direction. When observing from the inverter 1 port toward the neutral point of three-phase windings, the induced electromotive forces generated by suspension currents in U_1 and U_2 half-phase windings cancel out each other.

The expressions for the terminal voltage of other phase windings output by inverter 1 can be obtained similarly; this will not be further elaborated here.

3.2. Torque Modeling under MPSC-BI Method. In case of suspension current bilateral injection (MPSC-BI), in order to consider the influence of injected suspension current on the torque, according to the winding connection of MPI-BL-PMSM in Figure 2, relevant definitions are made as follows:

(1) $U_1, V_1,$ and W_1 constitute the first group of three-phase symmetrical "half-phase winding" coils, where the reference directions of torque current and suspension current are opposite.

(2) $U_2, V_2,$ and W_2 constitute the second group of three-phase symmetrical "half-phase winding" coils, where the reference directions of torque current and suspension current are the same.

Then, the instantaneous torque of MPI-BL-PMSM can be represented as the sum of the torques generated by two groups of "half-phase winding" coils.

Definition 1. d-q is the rotor magnetic field orientation synchronous coordinate system. Then by conducting vector transformations on the current equations and flux-linkage equations for two groups of three-phase symmetrical "half-phase winding" coils, respectively, the dynamic mathematical model in d-q coordinate system can be derived. The transformation matrix for two sets of "half-phase winding" coils from three-phase stationary coordinate system to d-q synchronous coordinate system is as follows:

$$
\begin{cases}
T = \begin{bmatrix} C & 0 \\[2mm] 0 & C \end{bmatrix}, \\[6mm]
C = \dfrac{2}{3} \begin{bmatrix} \cos \omega t & \cos\left(\omega t - \dfrac{2\pi}{3}\right) & \cos\left(\omega t + \dfrac{2\pi}{3}\right) \\[4mm] -\sin \omega t & -\sin\left(\omega t - \dfrac{2\pi}{3}\right) & -\sin\left(\omega t + \dfrac{2\pi}{3}\right) \end{bmatrix}.
\end{cases}
\tag{6}
$$

In equation (1), the coil current comprises torque- and suspension-current components. After performing coordinate transformation for equation (1) as follows:

$$
\begin{bmatrix} i_{d1} \\ i_{q1} \\ i_{d2} \\ i_{q2} \end{bmatrix} = T \begin{bmatrix} i_{u1} \\ i_{v1} \\ i_{w1} \\ i_{u2} \\ i_{v2} \\ i_{w2} \end{bmatrix},
\tag{7}
$$

the corresponding components of two sets of "three-phase symmetrical half winding" currents in the d-q synchronous coordinate system can be obtained, with specific expressions as follows:

$$
\left.\begin{aligned}
i_{d1} &= \frac{2}{3}\left\{\left[i_{Tu}\cos\omega t + i_{Tv}\cos\left(\omega t - \frac{2\pi}{3}\right) + i_{Tw}\cos\left(\omega t + \frac{2\pi}{3}\right)\right]\right. \\
&\quad \left. -\left[i_{Su}\cos\omega t + i_{Sw}\cos\left(\omega t - \frac{2\pi}{3}\right) + i_{Sv}\cos\left(\omega t + \frac{2\pi}{3}\right)\right]\right\} \\
i_{q1} &= \frac{2}{3}\left\{-\left[i_{Tu}\sin\omega t + i_{Tv}\sin\left(\omega t - \frac{2\pi}{3}\right) + i_{Tw}\sin\left(\omega t + \frac{2\pi}{3}\right)\right]\right. \\
&\quad \left. +\left[i_{Su}\sin\omega t + i_{Sw}\sin\left(\omega t - \frac{2\pi}{3}\right) + i_{Sv}\sin\left(\omega t + \frac{2\pi}{3}\right)\right]\right\} \\
i_{d2} &= \frac{2}{3}\left\{\left[i_{Tu}\cos\omega t + i_{Tv}\cos\left(\omega t - \frac{2\pi}{3}\right) + i_{Tw}\cos\left(\omega t + \frac{2\pi}{3}\right)\right]\right. \\
&\quad \left. +\left[i_{Su}\cos\omega t + i_{Sw}\cos\left(\omega t - \frac{2\pi}{3}\right) + i_{Sv}\cos\left(\omega t + \frac{2\pi}{3}\right)\right]\right\} \\
i_{q2} &= \frac{2}{3}\left\{-\left[i_{Tu}\sin\omega t + i_{Tv}\sin\left(\omega t - \frac{2\pi}{3}\right) + i_{Tw}\sin\left(\omega t + \frac{2\pi}{3}\right)\right]\right. \\
&\quad \left. -\left[i_{Su}\sin\omega t + i_{Sw}\sin\left(\omega t - \frac{2\pi}{3}\right) + i_{Sv}\sin\left(\omega t + \frac{2\pi}{3}\right)\right]\right\}
\end{aligned}\right\}. \tag{8}
$$

In equations (7) and (8), i_{d1} and i_{q1} are the d- and q-axis current components of the first group of three-phase symmetrical "half-phase winding" coils; i_{d2} and i_{q2} are the d-and q-axis current components of the second group of three-phase symmetrical "half-phase winding" coils.

Similarly, by coordinate transformation, the expressions of magnetic flux-linkage in d-q synchronous coordinate system are obtained for two sets of three-phase symmetrical "half-phase winding" as follows:

$$
\begin{bmatrix} \psi_{d1} \\ \psi_{q1} \\ \psi_{d2} \\ \psi_{q2} \end{bmatrix} = T \begin{bmatrix} \psi_{u1} \\ \psi_{v1} \\ \psi_{w1} \\ \psi_{u2} \\ \psi_{v2} \\ \psi_{w2} \end{bmatrix} = \begin{bmatrix} L_d & 0 & L_d & 0 \\ 0 & L_q & 0 & L_q \\ L_d & 0 & L_d & 0 \\ 0 & L_q & 0 & L_q \end{bmatrix} \begin{bmatrix} i_{d1} \\ i_{q1} \\ i_{d2} \\ i_{q2} \end{bmatrix} + \begin{bmatrix} \psi_f \\ 0 \\ \psi_f \\ 0 \end{bmatrix}, \tag{9}
$$

wherein L_d and L_q represent the d- and q-axis inductance of three-phase symmetrical "half-phase winding" in d-q synchronous coordinate system, $L_d = L_q = 3/2 * L_{mf}$.

The magnetic field energy storage within the stator winding of MPI-BL-PMSM can be expressed as follows:

$$
w_s = \frac{1}{2}\begin{bmatrix} i_{u1} & i_{v1} & i_{w1} & i_{u2} & i_{v2} & i_{w2} \end{bmatrix} \begin{bmatrix} \psi_{u1} \\ \psi_{v1} \\ \psi_{w1} \\ \psi_{u2} \\ \psi_{v2} \\ \psi_{w2} \end{bmatrix} = \frac{1}{2}\cdot\frac{3}{2}\begin{bmatrix} L_d\left(i_{d1} + i_{d2}\right)^2 + L_q\left(i_{q1} + i_{q2}\right)^2 \\ +\psi_f\left(i_{d1} + i_{d2}\right) \end{bmatrix}. \tag{10}
$$

Here, the permanent magnet flux-linkage is equivalent to the excitation current i_f in the rotor's equivalent excitation winding, i.e., "$\psi_f = L_{mf} i_f$" holds, where i_f is the equivalent current of permanent magnet. Then, according to the double reaction principle, the stator q-axis current always acts at the rotor's cross-axis position, and it does not generate magnetic flux-linkage in the rotor's equivalent excitation winding. On the other hand, the stator d-axis current always acts at the direct-axis position and produces magnetic flux-linkage in the rotor's equivalent excitation winding; this flux-linkage overlays with the permanent magnet flux-linkage. Therefore, the magnetic flux-linkage in rotor's equivalent excitation winding can be expressed as follows:

$$\psi_{r1} = \frac{3}{2} L_{mf} i_{d1} + L_{mf} i_f,$$
$$\psi_{r2} = \frac{3}{2} L_{mf} i_{d2} + L_{mf} i_f. \tag{11}$$

The magnetic field energy in the rotor's equivalent excitation winding can be expressed as follows:

$$w_r = \frac{1}{2} i_f \left(\psi_{r1} + \psi_{r2} \right) = \frac{1}{2} \cdot \frac{3}{2} \psi_f \left(i_{d1} + i_{d2} \right) + L_{mf} i_f^2. \tag{12}$$

By summing up the magnetic field energy in the stator winding and rotor winding, the total magnetic energy of MPI-BL-PMSM can be obtained as follows:

$$w = w_s + w_r$$
$$= \frac{3}{4} \left[L_d \left(i_{d1} + i_{d2} \right)^2 + L_q \left(i_{q1} + i_{q2} \right)^2 \right] \tag{13}$$
$$+ \frac{3}{2} \psi_f \left(i_{d1} + i_{d2} \right) + L_{mf} i_f^2.$$

From the electromechanical energy conversion principle, the electromagnetic torque is equal to the partial derivative of motor magnetic field energy relative to the mechanical angle θ_m. Then:

$$T_{em} = \frac{\partial w}{\partial \theta_m} = p_T \frac{\partial w}{\partial \alpha} = p_T \left(\frac{\partial w}{\partial i_{d1}} \cdot \frac{\partial i_{d1}}{\partial \alpha} + \frac{\partial w}{\partial i_{q1}} \cdot \frac{\partial i_{q1}}{\partial \alpha} + \frac{\partial w}{\partial i_{d2}} \cdot \frac{\partial i_{d2}}{\partial \alpha} + \frac{\partial w}{\partial i_{q2}} \cdot \frac{\partial i_{q2}}{\partial \alpha} \right)$$
$$= \frac{3}{2} p_T \left[\left(L_d - L_q \right) \left(i_{d1} + i_{d2} \right) \left(i_{q1} + i_{q2} \right) + \psi_f \left(i_{q1} + i_{q2} \right) \right]. \tag{14}$$

For the surface-mounted permanent magnet rotor structure, the d- and q-axis inductances are equal in the synchronous coordinate system. Then:

$$T_{em} = P_T \frac{\partial w}{\partial \alpha} = \frac{3}{2} P_T \psi_f \left(i_{q1} + i_{q2} \right). \tag{15}$$

In equation (15), P_T is the the number of magnetic poles in the torque system. By substituting it into equation (8), then the analytical expression for the electromagnetic torque Under MPSC-BI method can be obtained as follows:

$$T_{em} = \frac{3}{2} p_T \psi_f \left(i_{q1} + i_{q2} \right)$$
$$= -2 p_T \psi_f \left[i_{Tu} \sin \omega t + i_{Tv} \sin \left(\omega t - \frac{2\pi}{3} \right) + i_{Tw} \sin \left(\omega t + \frac{2\pi}{3} \right) \right] \tag{16}$$
$$= 3 P_T \psi_f I_T \sin \varphi_T.$$

Equation (16) indicates that when using the proposed MPSC-BI method, the suspension current components in i_{q1} and i_{q2} will mutually cancel out in the torque equation. This means that the suspension current will not affect the torque, which is more conducive to decoupling control between the torque system and suspension system.

3.3. Torque Modeling under MPSC-UI Method.

Compared with MPSC-BI method, when adopting suspension current unilateral injection (MPSC-UI), the suspension current is no longer superimposed in the upper "half-phase winding" of each phase, i.e., U_1, V_1, and W_1 half-phase windings in Figure 2 no longer contain suspension currents, and only U_2,

V_2, and W_2 half-phase windings are superimposed with suspension currents i_{su}, i_{sw}, and i_{sv}, respectively. Here, the current expressions of all half-phase windings are as follows:

$$
\begin{bmatrix} i_{u1} \\ i_{v1} \\ i_{w1} \\ i_{u2} \\ i_{v2} \\ i_{w2} \end{bmatrix} = \begin{bmatrix} i_{Tu} \\ i_{Tv} \\ i_{Tw} \\ i_{Tu} + i_{Su} \\ i_{Tv} + i_{Sw} \\ i_{Tw} + i_{Sv} \end{bmatrix} = I_T \begin{bmatrix} \cos(\omega t + \varphi_T) \\ \cos\left(\omega t - \dfrac{2\pi}{3} + \varphi_T\right) \\ \cos\left(\omega t + \dfrac{2\pi}{3} + \varphi_T\right) \\ \cos(\omega t + \varphi_T) \\ \cos\left(\omega t - \dfrac{2\pi}{3} + \varphi_T\right) \\ \cos\left(\omega t + \dfrac{2\pi}{3} + \varphi_T\right) \end{bmatrix} + I_S \begin{bmatrix} 0 \\ 0 \\ 0 \\ \cos(\omega t + \varphi_S) \\ \cos\left(\omega t + \dfrac{2\pi}{3} + \varphi_S\right) \\ \cos\left(\omega t - \dfrac{2\pi}{3} + \varphi_S\right) \end{bmatrix}. \tag{17}
$$

After performing coordinate transformation of equation (7), the current expressions in d-q synchronous coordinate system can be obtained as follows:

$$
\left.
\begin{aligned}
i_{d1} &= \frac{2}{3}\left[i_{Tu}\cos\omega t + i_{Tv}\cos\left(\omega t - \frac{2\pi}{3}\right) + i_{Tw}\cos\left(\omega t + \frac{2\pi}{3}\right)\right], \\[2mm]
i_{q1} &= -\frac{2}{3}\left[i_{Tu}\sin\omega t + i_{Tv}\sin\left(\omega t - \frac{2\pi}{3}\right) + \frac{1}{2}i_{Tw}\sin\left(\omega t + \frac{2\pi}{3}\right)\right], \\[2mm]
i_{d2} &= \frac{2}{3}\left\{\left[i_{Tu}\cos\omega t + i_{Tv}\cos\left(\omega t - \frac{2\pi}{3}\right) + i_{Tw}\cos\left(\omega t + \frac{2\pi}{3}\right)\right]\right. \\[2mm]
&\quad \left.+\left[i_{Su}\cos\omega t + i_{Sw}\cos\left(\omega t - \frac{2\pi}{3}\right) + i_{Sv}\cos\left(\omega t + \frac{2\pi}{3}\right)\right]\right\}, \\[2mm]
i_{q2} &= \frac{2}{3}\left\{-\left[i_{Tu}\sin\omega t + i_{Tv}\sin\left(\omega t - \frac{2\pi}{3}\right) + i_{Tw}\sin\left(\omega t + \frac{2\pi}{3}\right)\right]\right. \\[2mm]
&\quad \left.-\left[i_{Su}\sin\omega t + i_{Sw}\sin\left(\omega t - \frac{2\pi}{3}\right) + i_{Sv}\sin\left(\omega t + \frac{2\pi}{3}\right)\right]\right\}.
\end{aligned}
\right\}. \tag{18}
$$

Substituting (18) into (15), then the analytical expression for the electromagnetic torque under the MPSC-UI method can be obtained as follows:

$$T_{em} = \frac{3}{2} p\psi_f \left(i_{q1} + i_{q2}\right)$$

$$= -p\psi_f \left\{ 2\left[i_{Tu}\sin\omega t + i_{Tv}\sin\left(\omega t - \frac{2\pi}{3}\right)\right.\right.$$

$$\left. + i_{Tw}\sin\left(\omega t + \frac{2\pi}{3}\right) + \left[i_{Su}\sin\omega t \right.\right. \qquad (19)$$

$$\left.\left. + i_{Sw}\sin\left(\omega t - \frac{2\pi}{3}\right) + i_{Sv}\sin\left(\omega t + \frac{2\pi}{3}\right)\right]\right]\right\}$$

$$= 3P_T\psi_f I_T \sin\varphi_T - \frac{3}{2}P_T\psi_f I_S \sin\left(2\omega t + \varphi_S\right).$$

In equation (19), i_{su}, i_{sw}, and i_{sv} are the real-time values of three-phase symmetrical suspension currents injected from the midpoints of U, V, and W phase windings into the their lower "half-phase winding"; in the final expression, the first term "$3P_T\psi_f I_T \sin(\varphi_T)$" is the expression for controllable electromagnetic torque, and the second term "$1.5P_T\psi_f I_s \sin(2\omega t + \varphi_T)$" is the dynamic coupling torque generated by the suspension current.

By analyzing equations (16) and (19), the following research results are obtained:

(1) Compared with the MPSC-BI method, when the MPSC-UI method is adopted, because the suspension current component in i_{q2} cannot be canceled out in the torque equation again, the electromagnetic torque equation contains the coupling torque term generated by the suspension current, thereby exacerbating the torque's dynamic fluctuation.

(2) In the MPSC-UI case, the coupled torque has a clear dual-frequency characteristic, that is, the fluctuation frequency of the coupled torque is twice the rotational angular frequency of the synchronous magnetic field.

4. Torque Model Verification and Electromagnetic Coupling Characteristics Analysis

4.1. Body Model and Torque Ripple Characteristics of MPI-BL-PMSM.
Based on the ANSYS/Maxwell software, the body model of MPI-BL-PMSM is constructed. Figure 4 shows the 3-D sectional view and stator groove shape structure. Table 1 gives the motor's structural parameters.

The torque pulsation comprises two primary components: cogging torque and ripple torque. The cogging torque arises from the interaction between the permanent magnet and stator core when the winding is not energized, while the ripple torque results from the harmonic torque generated by the interaction between the stator's harmonic magnetic potential and the rotor's permanent magnet field.

During the MPI-BL-PMSM operation, each passage of permanent magnet through a stator slot induces a cogging torque fluctuation. As permanent magnet rotor completes one revolution, the cogging torque undergoes fluctuation NL times, where NL represents the least common multiple of motor pole-pairs and number of slots (here, NL = 12). In this paper, to mitigate cogging torque, the MPI-BL-PMSM employs an unequal-thickness permanent magnet pole structure by redesigning the tile-shaped permanent magnet to have different centers for inner and outer diameters, and the eccentric distance between the inner and outer centers of tile-shaped permanent magnet is set to 6 mm. Figure 5 depicts the cogging torque waveform of the MPI-BL-PMSM as a function of time (rotor position), and the fluctuation amplitude of cogging torque is 5.0 mN·m. The influence of cogging torque with this small fluctuation basically can be ignored.

After introducing torque current, the pulsation torque caused by torque current is derived by excluding the steady-state mean torque and cogging torque from the output torque. Figure 6 shows the dynamic variation waveform of ripple torque over time (rotor position) at 5.0 A torque current, featuring an amplitude of 50 mN·m. It is noteworthy that the ripple torque escalates with the increase in torque current, constituting the primary factor contributing to torque ripple in the motor analyzed in this study. The reason for the existence of obvious ripple torque is that the stator concentrated winding is used, and the stator magnetic potential contains a significant amount of harmonic magnetic potential.

4.2. Verification Analysis of Torque Model.
Under the conditions that the rotor is not eccentric and the suspension current is not injected, the torque characteristics of midpoint current injection type BL-PMSM is analyzed. Here, we set the torque current to take values in the range of 0~6 A with 1 A step size. Through FEM dynamic analysis, the dynamic waveform of the electromagnetic torque is obtained as a function of torque current and rotor position, as shown in Figure 7. Additionally, Figure 8 presents a comparison between the mean value of the FEM analysis waveform of electromagnetic torque and the calculated values from the mathematical model. From Figures 7 and 8, the following research results are obtained:

(1) Under the unsaturated magnetic circuit condition, the steady-state mean value of electromagnetic torque generally shows a proportional relationship with the torque current, and the results of FEM simulation experiments are basically consistent with the model calculation values. As an illustration, considering a torque current of 6 A, the results of FEM analysis indicate that the mean value of electromagnetic torque is 1.21 N·m, whereas the calculation value from the mathematical model is 1.27 N·m, and the error between them is 4.96%. The reason for the existence of errors is primarily attributed to the omission of factors such as copper loss and stray loss during the mathematical modeling for electromagnetic torque.

(2) Under different torque currents, the fluctuation frequency of electromagnetic torque with respect to rotor position remains constant, and the count of
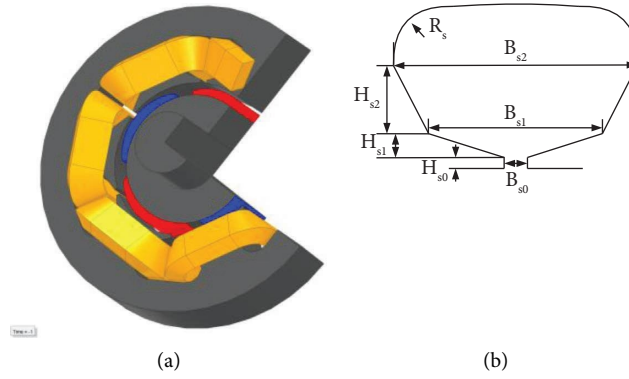
(a)   (b)

FIGURE 4: (a) 3-D sectional view and (b) stator slot shape.

TABLE 1: Structural parameters of MPI-BL-PMSM

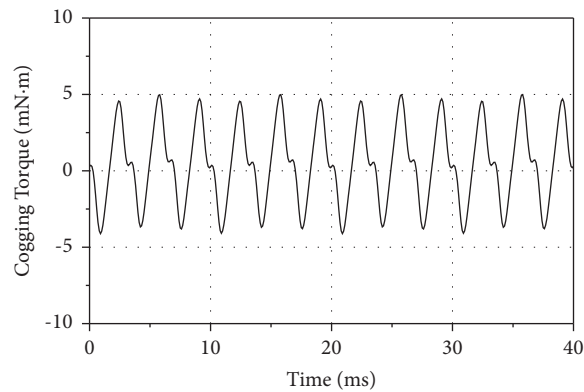| Parameters	Value
Stator slot count	6
Stator inner diameter (mm)	50
Stator outer diameter (mm)	100
Rotor outer diameter (mm)	42
Axial length (mm)	40
Air gap length (mm)	1
Winding turns count	50
PM thickness (mm)	3
PM material	NdFe35
PM remanence density (T)	1.23
PM flux-linkage Ψ_f (Wb)	0.0352
H_{s0} (mm)	1
H_{s1} (mm)	2
H_{s2} (mm)	6
B_{s0} (mm)	2
B_{s1} (mm)	15
B_{s2} (mm)	21
R_s (mm)	5

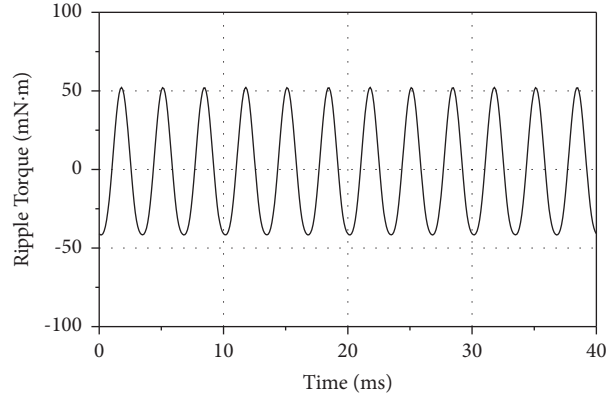FIGURE 5: Cogging torque waveform.

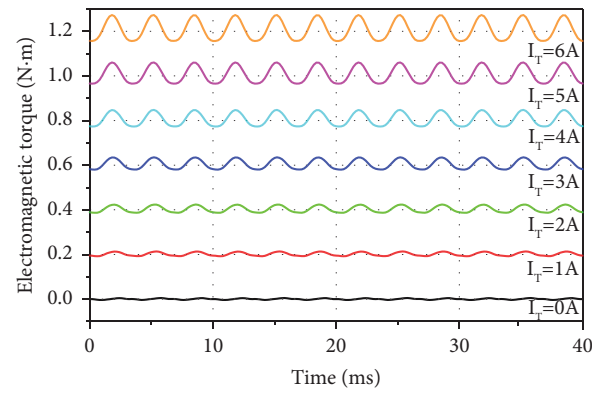FIGURE 6: Ripple torque waveform at 5.0 A torque current.

FIGURE 7: Dynamic waveform of electromagnetic torque.

fluctuations within one rotation cycle aligns with the fluctuations in cogging torque and ripple torque.

(3) The electromagnetic torque waveform is relatively stable. As the torque current increases, the steady-state mean torque and ripple torque generated by torque current are basically proportional changes, and the torque fluctuation rate varies between 9.13% and 9.61% (below 10%), which can meet the general application requirements.

4.3. Electromagnetic Coupling Characteristics Analysis of Injected Suspension Current on Torque. Under the rotor noneccentricity condition, the influences of injected suspension current on the electromagnetic torque of BL-PMSM for two different midpoint injection methods are investigated. Holding the torque current I_T as a constant of 5 A, making the suspension current superimposed on the coils (half-phase windings) within the range of 0–3 A at a step size of 0.5 A. Figures 9 and 10 present the dynamic FEM simulation waveforms of electromagnetic torque for the MPSC-BI method and MPSC-UI method, respectively. Figure 11 is the partial enlarged waveform of torque when using the MPSC-BI method. For convenience of comparing

waveform details, Figure 12 shows a comparison of torque waveforms between the two current injection methods when adding the same 3.0 A suspension current to the half-phase windings.

From Figures 9–12, the following results are obtained:

(1) Under the same torque current condition, whether the suspension current is injected unilaterally or bilaterally from the midpoint of each phase-winding, it does not affect the torque's steady-state mean. Here, with 5.0 A torque current, their steady-state mean values of torque are all approximately 1.01 Nm.

(2) Taking 5.0 A torque current as an example, and under the condition of adding 3 A suspension current on the "half-phase winding," the torque's "peak-to-peak differences" are 0.095 N and 0.66 N for the MPSC-BI and MPSC-UI methods, respectively. For MPSC-BI method, the torque fluctuation rate is 9.44%, which is basically the same as when there is no suspension current. For the MPSC-UI method, the torque fluctuation rate increases from 9.43% at zero suspension current to 64.88% at 3 A suspension current.
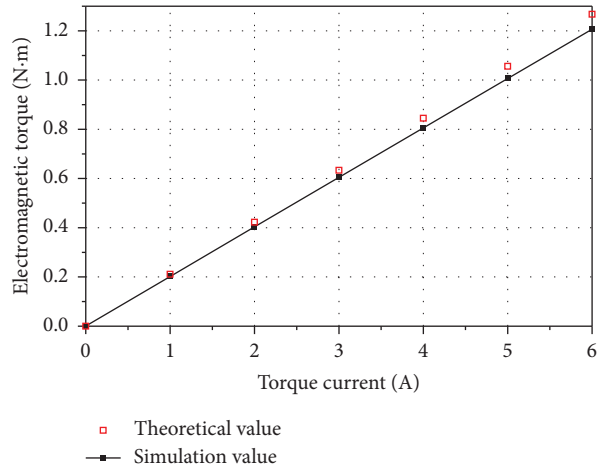
Figure 8: Value comparison curve of electromagnetic torque between FEM simulation and model calculation.
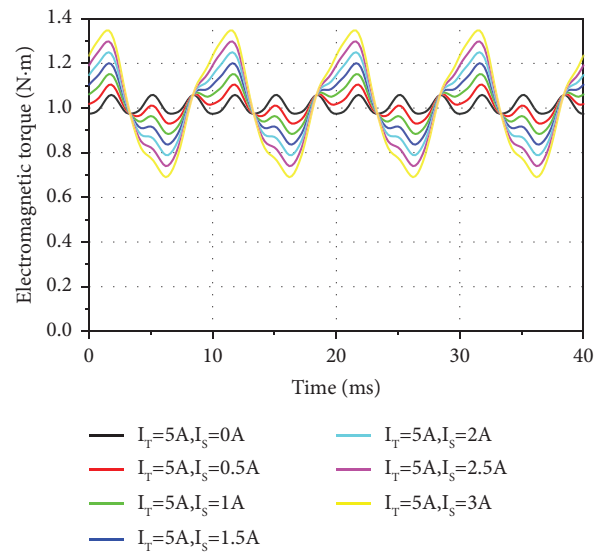

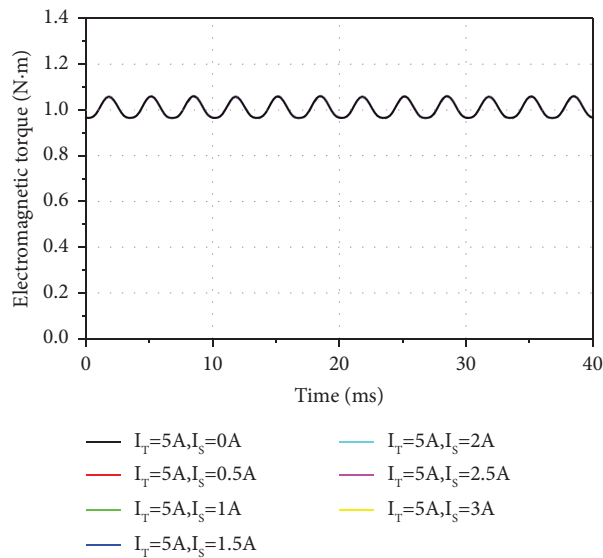Figure 9: Torque waveform under MPSC-UI method.

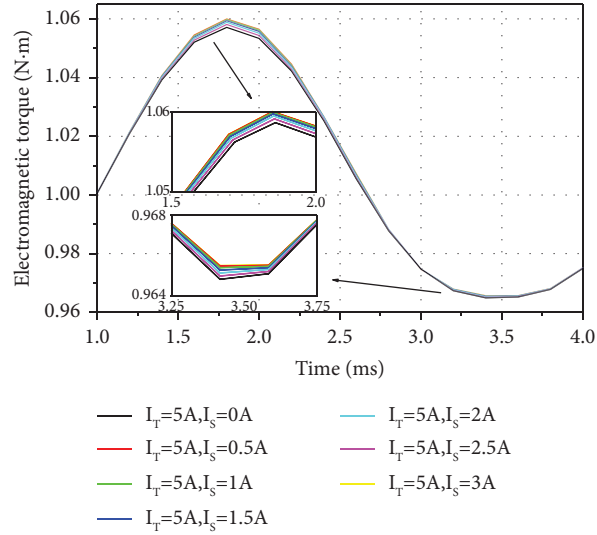Figure 10: Torque waveform under MPSC-BI method.

FIGURE 11: Enlarged torque waveform under MPSC-BI method.

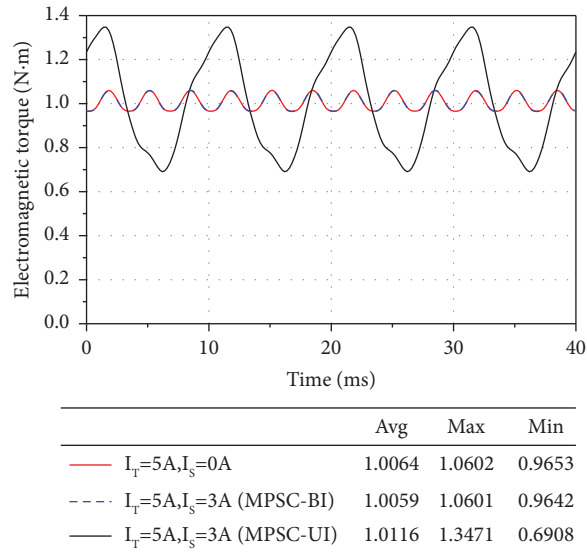|	Avg	Max	Min
I_T=5A,I_S=0A	1.0064	1.0602	0.9653
I_T=5A,I_S=3A (MPSC-BI)	1.0059	1.0601	0.9642
I_T=5A,I_S=3A (MPSC-UI)	1.0116	1.3471	0.6908

FIGURE 12: Torque waveform comparison between two suspension current injection methods.

(3) When using the MPSC-UI method, at each revolution of the rotor (40 ms), the four-pole permanent magnet field rotates 2 pairs of magnetic-pole ranges, and there are a total of 4 significant coupling torque pulsations in the torque waveform. The coupling pulsation frequency of torque is exactly twice the frequency of the magnetic field alternating frequency, thus verifying the "dual-frequency" characteristic of the suspension current coupling torque in the dynamic torque expression in equation (19).

When adopting the MPSC-UI method, the reason for the torque ripple increase is that the injected suspended current flows only in one "half-phase winding" of each phase, which results in a lack of symmetry in the magnetic flux distribution generated by suspension current. The pulsating torque generated by the interaction between an asymmetrically distributed suspension magnetic field and a torque magnetic field with different pole pairs cannot be canceled out, which inevitably results in an obvious increase in torque fluctuation amplitude. The coupled torque is basically proportional to the unilateral injection suspension current, and the FEM analysis results are consistent with equation (19). At this point, the coupling torque ripple waveform with a larger amplitude is not strictly a sine wave, as it also superimposes relatively smaller amplitude cogging torque and ripple torque.

(4) When using the MPSC-BI method, the torque fluctuation is basically unaffected by the injected suspension current, or minimally affected. In this case, the "peak to peak" fluctuation rate of torque
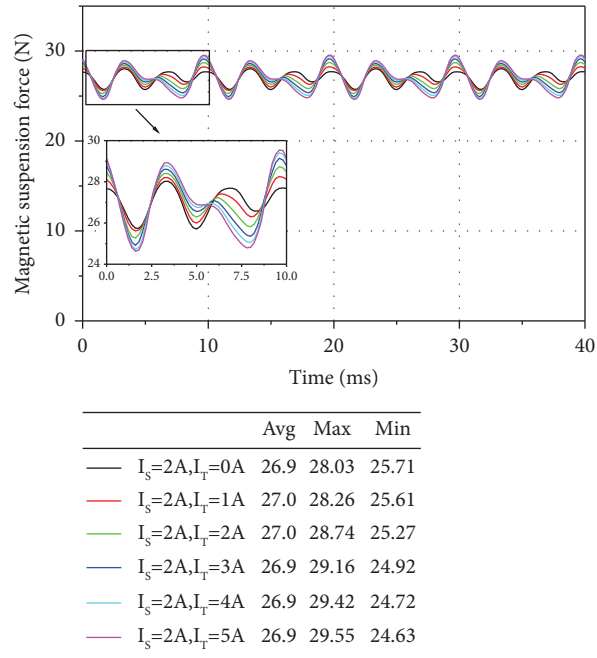
	Avg	Max	Min
—— I_S=2A,I_T=0A	26.9	28.03	25.71
—— I_S=2A,I_T=1A	27.0	28.26	25.61
—— I_S=2A,I_T=2A	27.0	28.74	25.27
—— I_S=2A,I_T=3A	26.9	29.16	24.92
—— I_S=2A,I_T=4A	26.9	29.42	24.72
—— I_S=2A,I_T=5A	26.9	29.55	24.63

FIGURE 13: Radial suspension force waveforms with torque current under MPSC-BI method.

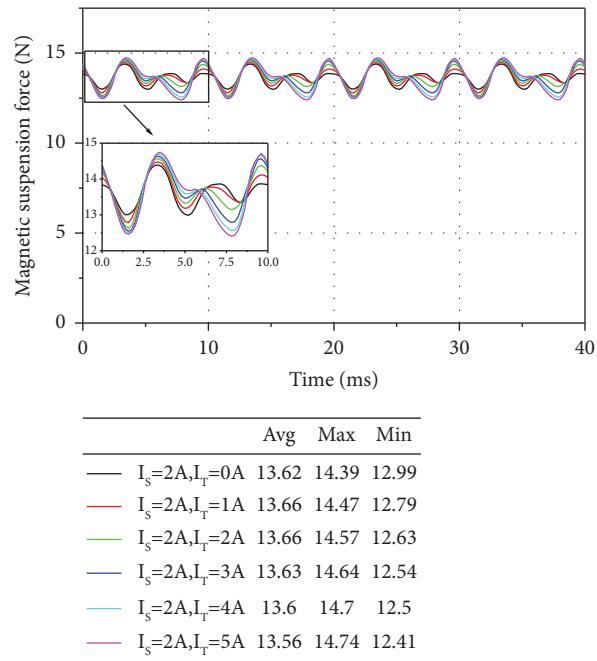|	Avg	Max	Min
—— I_S=2A,I_T=0A	13.62	14.39	12.99
—— I_S=2A,I_T=1A	13.66	14.47	12.79
—— I_S=2A,I_T=2A	13.66	14.57	12.63
—— I_S=2A,I_T=3A	13.63	14.64	12.54
—— I_S=2A,I_T=4A	13.6	14.7	12.5
—— I_S=2A,I_T=5A	13.56	14.74	12.41

FIGURE 14: Radial suspension force waveforms with torque current under MPSC-UI method.

remains around 9.4%, which is the advantage of the MPSC-BI method proposed in this paper. The results of FEM simulation analysis are consistent with equation (16). In Figure 10, with the suspension current change, there are slight variations of torque waveform's positive peak value ($\leq$2.8 m·N·m) and negative peak value ($\leq$0.8 m·N·m), and the slight variations are due to the additional ripple torque caused by injected suspension current, which can be ignored due to relatively too small value.

In Figures 9–11, the torque fluctuation at zero suspension current is attributed to the cogging torque and torque system ripple torque.

4.4. Electromagnetic Coupling Characteristics Analysis of Torque Current on Controllable Suspension Force. Now, under rotor noneccentricity condition, the coupling effect of torque current on the controllable magnetic suspension force will be analyzed for the two midpoint injection methods of suspension current. Here, maintaining the suspension current in the "half-phase winding" constant ($I_S = 2A$) and setting the torque current to take values at a step of 1 A within the range of 0–5 A, the dynamic FEM simulation response waveforms of controllable magnetic suspension force when adopting MPSC-BI and MPSC-UI methods are shown in Figures 13 and 14, respectively.

From Figures 13 and 14, the following results are obtained:

(1) Under the same condition of "half-phase winding" suspension current, the mean value of generated controllable magnetic suspension force when using the MPSC-BI method is approximately twice that when using the MPSC-UI method. Furthermore, under both injection methods of suspension current, the dynamic variation rules of generated controllable suspension force with time (or rotor position angle) are completely consistent.

(2) Whether MPSC-BI method or MPSC-UI method, torque current will enhance the fluctuation of controllable magnetic suspension force. Under the same condition of "half-phase winding" suspension current, when using the MPSC-BI method, the coupling effect of torque current on suspension force is slightly greater that that when using the MPSC-UI method.

Taking the suspension current "$I_S = 2A$" as an example, when the MPSC-BI method and MPSC-UI are used separately, the "peak-to-peak" differences of suspension force are 2.32 N and 1.40 N at zero torque current, with steady-state mean values of 26.99 N and 13.62 N, respectively. After applying a 5 A torque current, when the MPSC-BI method and MPSC-UI method are used separately, the "peak-to-peak" differences of suspension force are 4.92 N and 2.33 N, with steady-state mean values of 26.92 N and 13.56 N, respectively. Therefore, when using the MPSC-BI method, the "peak-to-peak" fluctuation rate increment of suspension force is about 9.7%, slightly more than that of 6.9% when using the MPSC-UI method. This effect primarily originates from the coupling influence of torque system's harmonic magnetic potential on the radial suspension force. For the practical control systems of BL-PMSM equipped with radial displacement closed-loop controllers, such coupling effects can be effectively suppressed.

5. Conclusion

In this paper, the MPI-BL-PMSM is taken as study object, an MPSC-BI method is proposed, the in-depth modeling research and coupling characteristic analysis on its torque system have been conducted, and the mathematical model of electromagnetic torque is analytically derived. From the perspectives of theoretical methodical mode analysis and finite element simulation experiment, the advantages of torque characteristics have been demonstrated for the proposed MPSC-BI method. Research conclusions are as follows:

(1) The electromagnetic torque mathematical model established based on the basic mathematical models of two sets of three-phase symmetrical "half-winding" is correct. Under the unsaturated magnetic circuit condition, the relationship between torque current and steady-state torque amplitude is essentially linear.

(2) When using the MPSC-UI method, the injected suspension current will couple to produce a "dual-frequency" pulsating torque with a large amplitude. As the suspension current increases, the amplitude of coupling torque will also increase, which is very unfavorable for the dynamic suspension control of the rotor.

(3) Under the same torque current condition, when using the proposed MPSC-BI method, the coupling effect of injected suspension current on the electromagnetic torque is much smaller than that when adopting the MPSC-UI method. Based on the proposed MPSC-BI method, the torque pulsation caused by the injected suspension current can be effectively suppressed or avoided, and the dynamic stability of torque waveform can be effectively improved.

(4) Under the same "half-phase winding suspension current" condition, when adopting the proposed MPSC-BI method, the steady-state mean of generated controllable magnetic suspension force is approximately twice that when adopting the MPSC-UI method. For the MPSC-BI method, the coupling effect of torque current on the radial magnetic suspension force is slightly greater than that of the MPSC-UI method.

Data Availability

The data used to support the findings of this study are available from the corresponding author upon request.

Conflicts of Interest

The authors declare that they have no conflicts of interest.

Acknowledgments

References

[1] S. S. Badini and V. Verma, "Parameter independent speed estimation technique for PMSM drive in electric vehicle," *International Transactions on Electrical Energy Systems*, vol. 31, no. 11, 2021.

[2] R. Taniguchi, S. Ishida, K. Yagi, and S. Ohashi, "Analysis of the amount of flux variation on the HTS surface by the oscillation of HTS magnetic bearing rotor," *IEEE Transactions on Magnetics*, vol. 59, no. 11, pp. 1–4, 2023.

[3] T. Pei, D. Li, J. Liu, J. Li, and W. Kong, "Review of bearingless synchronous motors: principle and topology," *IEEE Transactions on Transportation Electrification*, vol. 8, no. 3, pp. 3489–3502, 2022.

[4] F. Ahmed, K. Kalita, and H. B. Nemade, "Torque and controllable radial force production in a single winding bearingless switched reluctance motor with a speed controlled drive operation," *International Transactions on Electrical Energy Systems*, vol. 30, no. 5, 2020.

[5] Z.-B. Yang, P.-J. Jia, X.-D. Sun, and H.-T. Mei, "Rotor vibration unbalance compensation control of a bearingless induction motor," *International Transactions on Electrical Energy Systems*, vol. 31, no. 8, 2021.

[6] Q.-W. Xiang, Y. Ou, Z.-D. Peng, and Y.-K. Sun, "Review on self-decoupling topology of bearingless switched reluctance motor," *Energies*, vol. 16, no. 8, p. 3492, 2023.

[7] K. Xu, Y.-G. Guo, G. Lei, X.-D. Sun, and J.-G. Zhu, "Electromagnetic performance analysis of a bearingless permanent magnet synchronous motor by model order reduction," *IEEE Transactions on Magnetics*, vol. 59, no. 11, pp. 1–5, 2023.

[8] J. Zhu, Z. Deng, X. Wang, and Q. Liao, "Design and realization of single winding bearingless slice motor power system," *Electric Machines and Control*, vol. 12, no. 1, pp. 5–9, 2008.

[9] A. Chiba, K. Sotome, Y. Iiyama, and M. A. Rahman, "A novel middle point current injection type bearingless PM synchronous motor for vibration suppression," *IEEE Transactions on Industry Applications*, vol. 47, no. 4, pp. 1700–1706, 2011.

[10] J. Huang, B. Li, H. Jiang, and M. Kang, "Analysis and control of multiphase permanent-magnet bearingless motor with a single set of half-coiled winding," *IEEE Transactions on Industrial Electronics*, vol. 61, no. 7, pp. 3137–3145, 2014.

[11] D. Dietz, G. Messager, and A. Binder, "1 kW/60,000 min^{-1}bearingless PM motor with combined winding for torque and rotor suspension," *IET Electric Power Applications*, vol. 12, no. 8, pp. 1090–1097, 2018.

[12] R. Oishi, S. Horima, H. Sugimoto, and A. Chiba, "A novel parallel motor winding structure for bearingless motors," *IEEE Transactions on Magnetics*, vol. 49, no. 5, pp. 2287–2290, 2013.

[13] E. L. Severson, R. Nilssen, T. Undeland, and N. Mohan, "Design of dual-purpose No-voltage combined windings for bearingless motors," *IEEE Transactions on Industry Applications*, vol. 53, no. 5, pp. 4368–4379, 2017.

[14] N. Petersen, A. Khamitov, T. Slininger, and E. L. Severson, "Machine design and precision current regulation for the parallel DPNV bearingless motor winding," *IEEE Transactions on Industry Applications*, vol. 57, no. 6, pp. 7000–7011, 2021.

[15] J. Asama and A. Chiba, "Three-coil combined winding configuration for a 2-DOF actively controlled bearingless permanent magnet motor," *IEEE Transactions on Industry Applications*, vol. 57, no. 6, pp. 6765–6773, 2021.

[16] W. W. Geng and Z. R. Zhang, "Investigation of a new ironless-stator self-bearing axial flux permanent magnet motor," *IEEE Transactions on Magnetics*, vol. 52, no. 7, pp. 1–4, 2016.

[17] W. Xiaoyuan, L. Na, Y. Tian, and L. Tianyuan, "Study on the effect of suspension windings on the electromagnetic vibration and noise of ultra-high-speed bearingless permanent magnet synchronous motor for air compressor," *IEEJ Transactions on Electrical and Electronic Engineering*, vol. 18, no. 1, pp. 129–138, 2023.